Confined Fe–Cu Clusters as Sub-Nanometer Reactors for Efficiently Regulating the Electrochemical Nitrogen Reduction Reaction

Xiaowei Wang
University of Wollongong, xww940@uowmail.edu.au

Siyao Qiu

Jianmin Feng

Yueyu Tong
University of Wollongong, yt932@uowmail.edu.au

Fengling Zhou

See next page for additional authors

Recommended Citation

Confined Fe–Cu Clusters as Sub-Nanometer Reactors for Efficiently Regulating the Electrochemical Nitrogen Reduction Reaction

Abstract

© 2020 The Authors. Published by Wiley-VCH GmbH Electrochemical nitrogen reduction reaction (NRR) over nonprecious-metal and single-atom catalysts has received increasing attention as a sustainable strategy to synthesize ammonia. However, the atomic-scale regulation of such active sites for NRR catalysis remains challenging because of the large distance between them, which significantly weakens their cooperation. Herein, the utilization of regular surface cavities with unique microenvironment on graphitic carbon nitride as "subnano reactors" to precisely confine multiple Fe and Cu atoms for NRR electrocatalysis is reported. The synergy of Fe and Cu atoms in such confined subnano space provides significantly enhanced NRR performance, with nearly doubles ammonia yield and 54%-increased Faradic efficiency up to 34%, comparing with the single-metal counterparts. First principle simulation reveals this synergistic effect originates from the unique Fe–Cu coordination, which effectively modifies the N2 absorption, improves electron transfer, and offers extra redox couples for NRR. This work thus provides new strategies of manipulating catalysts active centers at the sub-nanometer scale.

Disciplines

Engineering | Science and Technology Studies

Publication Details

Authors

Xiaowei Wang, Siyao Qiu, Jianmin Feng, Yueyu Tong, Fengling Zhou, Qinye Li, Li Song, Shuangming Chen, Kuang Wu, Panpan Su, Sheng Ye, Feng Hou, Shi Xue Dou, Hua-Kun Liu, Gao Lu, Chenghua Sun, Jian Liu, and Ji Liang

COMMUNICATION

ADVANCED
MATERIALS

www.advmat.d

Check for
updates

Confined Fe–Cu Clusters as Sub-Nanometer Reactors for Efficiently Regulating the Electrochemical Nitrogen Reduction Reaction

Xiaowei Wang, Siyao Qiu, Jianmin Feng, Yueyu Tong, Fengling Zhou, Qinye Li, Li Song, Shuangming Chen, Kuang-Hsu Wu, Panpan Su, Sheng Ye, Feng Hou, Shi Xue Dou, Hua Kun Liu, Gao Qing (Max) Lu, Chenghua Sun,* Jian Liu,* and Ji Liang*

Electrochemical nitrogen reduction reaction (NRR) over nonprecious-metal and single-atom catalysts has received increasing attention as a sustainable strategy to synthesize ammonia. However, the atomic-scale regulation of such active sites for NRR catalysis remains challenging because of the large distance between them, which significantly weakens their cooperation. Herein, the utilization of regular surface cavities with unique microenvironment on graphitic carbon nitride as "subnano reactors" to precisely confine multiple Fe and Cu atoms for NRR electrocatalysis is reported. The synergy of Fe and Cu atoms in such confined subnano space provides significantly enhanced NRR performance, with nearly doubles ammonia yield and 54%-increased Faradic efficiency up to 34%, comparing with the single-metal counterparts. First principle simulation reveals this synergistic effect originates from the unique Fe–Cu coordination, which effectively modifies the N_2 absorption, improves electron transfer, and offers extra redox couples for NRR. This work thus provides new strategies of manipulating catalysts active centers at the sub-nanometer scale.

Ammonia is traditionally an essential chemical for fertilizers and other nitrogen-containing products that have been supporting most of the world population for over a century. Recently, ammonia is receiving renascent attentions as a potential hydrogen storage medium and carbon-free fuel, due to its advantages of easy liquefaction to achieve a higher volumetric energy density and more facile transportation as compared with other gas-based fuels.[1] Conventionally, the industry-scale production of ammonia, based on the Habor–Bosch method through a nitrogen reduction reaction (NRR), is high-cost, energy-intensive, and environmentally unfriendly, as it not only consumes a large amount of fossil energy but also is associated with the release of

X. Wang, Prof. F. Hou, Prof. J. Liang
Key Laboratory for Advanced Ceramics and Machining Technology
of Ministry of Education
School of Materials Science and Engineering
Tianjin University
Tianjin 300350, China
E-mail: liangji@tju.edu.cn

X. Wang, Dr. J. Feng
Applied Physics Department
College of Physics and Materials Science
Tianjin Normal University
No. 393 Binshui West Road, Xiqing District, Tianjin 300387, China

X. Wang, Y. Tong, Prof. S. X. Dou, Prof. H. K. Liu,
Prof. J. Liang
Institute for Superconducting and Electronic Materials
University of Wollongong
Wollongong, NSW 2522, Australia

Dr. S. Qiu, Dr. F. Zhou
Science & Technology Innovation Institute
Dongguan University of Technology
Dongguan 523000, China

Q. Li, Prof. C. Sun
Department of Chemistry and Biotechnology, and Centre for
Translational Atomaterials
FSET
Swinburne University of Technology
Hawthorn, Victoria 3122, Australia
E-mail: chenghuasun@swin.edu.au

Prof. L. Song, Dr. S. Chen
National Synchrotron Radiation Laboratory
CAS Center for Excellence in Nanoscience
University of Science and Technology of China
Hefei, Anhui 230029, China

Dr. K.-H. Wu
School of Chemical Engineering
The University of New South Wales
Kensington, Sydney, NSW 2052, Australia

Dr. P. Su, Dr. S. Ye, Prof. J. Liu
State Key Laboratory of Catalysis
Dalian Institute of Chemical Physics
Chinese Academy of Sciences
457 Zhongshan Road, Dalian 116023, China
E-mail: jian.liu@surrey.ac.uk

Prof. G. Q. (M.) Lu, Prof. J. Liu
DICP-Surrey Joint Centre for Future Materials
Department of Chemical and Process Engineering, and Advanced
Technology Institute
University of Surrey
Guilford, Surrey GU2 7XH, UK

**ADVANCED
SCIENCE NEWS**
www.advancedsciencenews.com

**ADVANCED
MATERIALS**
www.advmat.de

carbon mono/dioxides during the reforming of methane to produce hydrogen.[2] Therefore, the development of sustainable strategies that produce ammonia is important. To address this, a variety of alternative methods have been proposed, including enzymatic, photo- and electrocatalysis, as well as chemical looping processes.[3]

As a strategy of ammonia synthesis utilizing H_2O as the hydrogen source, electrochemical reduction of N_2 to NH_3 is uniquely advanced because this mild progress can be facilely implemented under ambient conditions and potentially accompanied by a high energy conversion efficiency.[4] In an electrochemical NRR process, the electrocatalysts play the key role in accelerating the reaction rate and selectivity/efficiency. Thus, the exploration of efficient catalysts for NRR has drawn particular attraction in recent years.[5] By far, a number of catalysts that are based on metals (e.g., Ru,[6] Pd,[7] and Au[8]), oxides (e.g., Fe_2O_3/carbon nanotube,[9] $W_{18}O_{49}$,[10] and BiOBr nanosheets[11]), sulfides (e.g., FeMoS [12]), black phosphorus,[13] nitrides (e.g., C_3N_4 [14] and MoN [15]), carbides (MoC [16]), MXenes,[17] and single atoms (e.g., Mo,[18] B,[19] W,[20] and Ru [21]) have been investigated.

Among them, single-atom catalysts, in particular, the non-precious and transition-metal-based ones with unsaturated coordination features, are desirable for adsorbing nitrogen molecules due to their lowly coordinated electronic structure and efficient utilization of the active species.[18,19,22] Conceptually, in order to anchor the single atoms on the carrier surface and prevent them from aggregating, strong coordination to the substrate is essential.[19a,22g] Conventionally, these single metal atoms are "trapped" in the vacancy sites of carbon surface to maintain their stability; however, it still remains a challenge to increase the loading amount of single atom catalyst.[23] To further increase their loading amount and stability, a secondary (nonmetal) element has been introduced. For example, the nitrogen dopants in the carbon framework can provide stronger binding with the metal atoms by forming the metal–nitrogen covalent bonds, resulting in better dispersed single atoms at a higher amount.[19b,22e,24]

Despite these merits, two major obstacles still exist on these single-atom catalysts for further enhancing their performance. On the one hand, the distance between these single-atom catalytic centers, even though only a few nanometers, is still too far to be capable of cooperatively functioning for NRR, which requires to further decrease the interatom distance until 0.1–0.2 nm to the bond length of N≡N.[25] Theoretical works have predicted the possible cooperation of multiple atoms in small clusters for NRR catalysts,[26] however, the actual manipulation of the cluster's configuration is still fairly difficult and only very rare cases have been reported for the catalytic reactions other than NRR.[27] On the other hand, the quasi-semiconducting surface of these catalysts, which is caused by the metal/nonmetal coordination manner (e.g., $Fe-N_x$ or $Co-N_x$),[19a,22f] is also doubtable to provide sufficient electron transfer capability for the multielectron NRR process or other electrochemical catalysis, which can be the potential bottleneck for NRR but has been rarely noticed as well.

Recently, the nanoreactors, which commonly have an internal cavity that is capable of encapsulating multiple active species and reactants inside it, have shown significant advantages for accelerating a range of catalytic processes.[28] Such confinement not only provides better interaction between the reactants and the catalytic active species, but also, more importantly, leads to potential synergetic effect due to its unique microenvironments and the intimate contact between multiple active species, which is highly favorable for catalysis, especially the tandem processes such as NRR.[29] Consequently, it is desirable for the construction of novel "reactors" to confine single-atom catalytic centers within extremely close distance, it would probably solve the abovementioned issues of the current single-atom catalysts for NRR, which has unfortunately not yet been achieved by far.

Based on these considerations, we herein propose a proof of concept strategy of extending "nano reactors" to "subnano reactors" by confining multiple Fe and Cu atoms in the extremely narrow yet regular surface cavities of graphitic carbon nitride (denoted $CNT@C_3N_4$–Fe&Cu) for high-efficiency NRR electrocatalysis. In such atomic reactors, the Fe and Cu atoms simultaneously coordinate with each other and the surrounding N atoms, which can not only modify their electronic structures to anchor N_2 molecules/intermediates with optimized strength but also offer the capacity to cache electrons for rapid electron transfer, thus lowing the NRR barrier and significantly enhancing the NRR performance in terms of ammonia yield or Faradic efficiency.

The fabrication of $CNT@C_3N_4$–Fe&Cu is illustrated in **Figure 1**a and Figure S1 (Supporting Information). First, multiwalled carbon nanotubes (CNTs), as a conducting substrate, were mildly oxidized to form a better affinity with dicyandiamide (DICY) precursor and metal salts ($FeCl_2$ and $CuCl_2$ with a molar ratio of 1:1) in an aqueous solution. Then, the precursor solution was lyophilized, yielding the CNTs@DICY@ metal salts intermediate product. It was subsequently annealed in an inert atmosphere to form the final $CNT@C_3N_4$–Fe&Cu material. During this process, DICY polymerized into ultrathin C_3N_4 sheets, which have regular surface cavities with nitrogen atoms on their edge to bind with the metal atoms, forming the subnano reactors with multiple metal atoms inside them. For comparison, analogs were also fabricated by introducing mono ($CNT@C_3N_4$–Fe or –Cu) or no metal salts ($CNT@C_3N_4$) during fabrication (details in the Supporting Information).

The morphology and chemistry of the materials were first studied under transmission electron microscopy (TEM). The typical $CNT@C_3N_4$–Fe&Cu shows a similar hollow tubular morphology to pristine CNTs, without an obvious increment in diameter (Figure 1b; Figure S2a,b, Supporting Information). As revealed by energy disperse spectroscopy (EDS) mapping (Figure 1c–f), carbon is distributed throughout the whole area, while homogeneous Cu, Fe, and N signal can be found predominantly on the outer surface of the material to form a thin shell (1–2 nm), indicating their coaxial distribution. This is further confirmed by the electron energy loss spectroscopy (EELS), from which carbon can be found in both the surface and internal sections (I and II in Figure 1b), but with remarkable differences in their chemical structures. The surface carbon is amorphous without graphitic structure, corresponding to the poorly crystalized C_3N_4 (Figure 1g),[30] while the internal carbon shows typical graphitic features, assigned as CNTs (Figure 1h). Besides, nitrogen can only be detected on the surface, supporting the existence of a thin C_3N_4 layer outside
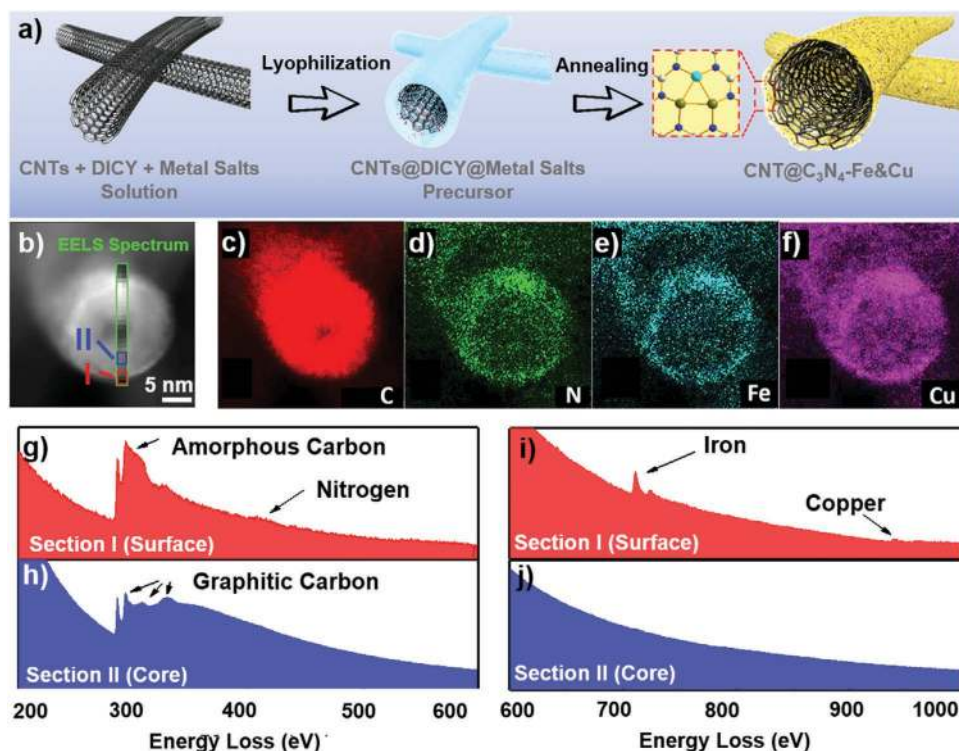
ADVANCED
SCIENCE NEWS

www.advancedsciencenews.com

ADVANCED
MATERIALS

www.advmat.de

Figure 1. Schematic diagram of synthesis and morphology of CNT@C_3N_4–Fe&Cu. a) Schematic diagram of synthesis and morphology of the CNT@C_3N_4–Fe&Cu; b) dark-field TEM image of the cross-section of CNT@C_3N_4–Fe&Cu; c–f) the corresponding elemental mapping of carbon, nitrogen, iron, and copper; EELS spectra of carbon of area g) I and h) II in (b); EELS spectra of i) Fe and j) Cu of areas I and II in (b).

the CNTs. Meanwhile, Fe and Cu also only exist on the surface (Figure 1i,j), in good agreement with the elemental mappings. This comprehensively confirms that a uniform C_3N_4 layer dual-doped Fe and Cu has been formed on the surface of CNTs.

The fine structure of CNT@C_3N_4-Fe&Cu and analogs was subsequently investigated by X-ray diffraction (XRD) and scanning transmission electron microscopy (STEM, **Figure 2**; Figures S3–S8, Supporting Information). XRD patterns of all these samples only show one peak at ≈26° (Figure S3,

Supporting Information), a typical feature of graphitic CNTs, which also indicates no crystalline metal or metal compounds was formed.[30] From STEM images, clear graphitic structures can be seen inside the material, corresponding to the CNTs (Figure 2a). Outside CNTs, a fur-like thin shell without any graphitic textures can be observed, corresponding to the C_3N_4 shell.

Under high resolution, numerous compact bright spots can be found homogeneously distributed on the surface of

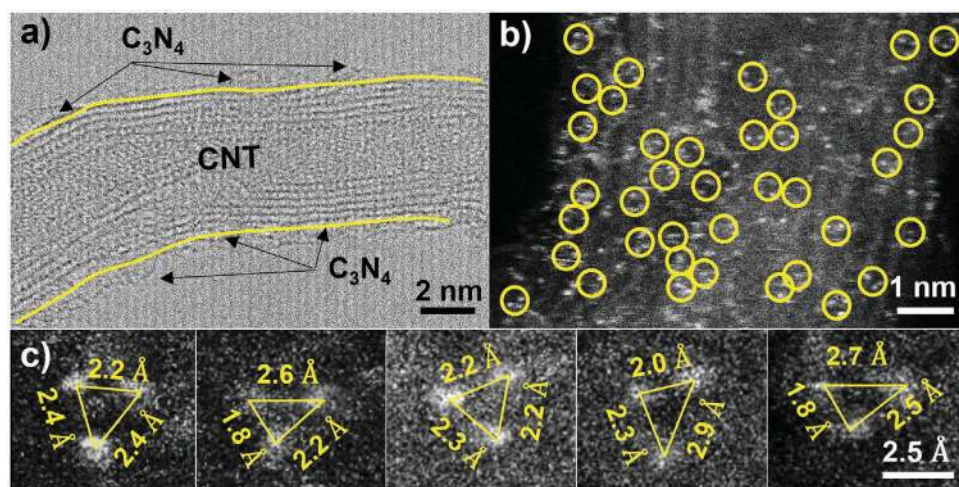**Figure 2.** Structural characterization of CNT@C_3N_4–Fe&Cu. a) TEM image of CNT@C_3N_4–Fe&Cu; b) STEM image of CNT@C_3N_4–Fe&Cu at high resolution; and c) STEM image of CNT@C_3N_4–Fe&Cu showing the triplet distribution of metal atoms and the distance between them.

the material, indicating their single-atom features (Figure 2b). Remarkably, it is very interesting to find a large portion of these atoms are in a triplet form, in which three metal atoms are very close to each other with an average distance of 1.8–2.5 Å (Figure 2c; Figures S5f and S7e, Supporting Information), with the rest being in doublet or single-atom form, while the comparative sample without C_3N_4 substrate shows typical single-atom features (Figure S6, Supporting Information). The geometry of such clusters fits well with the in-plane voids of g-C_3N_4, which is triangle-shaped with a side length of ≈4.8 Å, clearly suggesting their effective anchoring capability for single atoms to form subnano reactors with a closely confined configuration (details will be discussed later). More importantly, this ultrasmall interatom distance is close to the value in FeCu alloy (2.56 Å),[31] which is essential for not only the cooperation of individual single atoms for NRR electrocatalysis but also more facile electron transfer due to the significant metal–metal interaction in such subnano reactors.

The surface chemistry of the material was also studied by EELS. Figure S4 (Supporting Information) shows EELS spectra of the area in Figure 2b for C, N, Fe, and Cu, from which an enlarged Fe spectrum (Figure S4b, Supporting Information) has been derived and two peaks appear at around 710 eV, due to the electron transition from 2p to unoccupied 3d orbital.[32] Besides, a protuberance-like peak, which can be attributed to Cu, can also be observed at about 940 eV (Figure S4c, Supporting Information).[32b–d] This again confirms the coexistence of Fe and Cu atoms in the area. In contrast, only clean surface without metal atoms can be seen on CNT@C_3N_4 (Figure S9, Supporting Information). The STEM EDS spectra of the observed regions in the STEM images illustrated that the atomic react centers are neat and not polluted by the impurities

from the environment (Si, Na, Cl). Only corresponding Fe or Cu peaks were acquired in the CNT@C_3N_4–Fe or CNT@C_3N_4–Cu. Besides, The Fe:Cu ratio in CNT@C_3N_4–Fe&Cu (1.1:1) is close to its theoretical value (1:1), indicating a uniform dispersion of the atoms in the binary system. We have conducted the ICP tests to further confirm the Fe and Cu content in CNT@C_3N_4–Fe&Cu. As shown in Table S3 (Supporting Information), the content of Fe and Cu species in CNT@C_3N_4–Fe&Cu is 7.51% and 10.77%, close the estimated value (Fe ≈ 7.0%, Cu ≈ 7.81%).

The local coordination of atoms in such subnano reactors was then probed using X-ray absorption fine structure (XAFS), X-ray photoelectron spectroscopy (XPS), and EELS (**Figure 3**a,b; Figures S9–S11, Supporting Information). FePc and CuPc, with typical Cu/Fe–N_4 coordination structures, were used as reference. In the K-edge X-ray absorption near edge structure (XANES) spectra, the absorption edge of CNT@C_3N_4–Fe&Cu locates higher than Fe/CuPc, indicating a higher oxidation state of Fe and Cu. Interestingly, the first rising peak in the Fe and Cu XANES spectra of CNT@C_3N_4–Fe&Cu is lower than that of CNT@C_3N_4–Fe and CNT@C_3N_4–Cu, indicating a lower density of free electron in the d orbital of CNT@C_3N_4–Fe&Cu (Figure S9a,b, Supporting Information). The Fourier-transformed Fe/Cu k^3-weighted EXAFS R-space spectra of Fe and Cu in CNT@C_3N_4–Fe&Cu. In contrast, monometallic CNT@C_3N_4–Fe/Cu show similar peaks in the range of first shell, but significant difference in the second shell (Figure 3a,b). The spectra of CNT@C_3N_4–Fe&Cu is much neater compared with the monometal counterparts, indicating the fewer coordination structure in higher shells. The first-shell fitting of the K-edge Fourier transform results in CNT@C_3N_4–Fe&Cu, CNT@C_3N_4–Fe, CNT@C_3N_4–Cu, FePc, and CuPc (Figure 3;
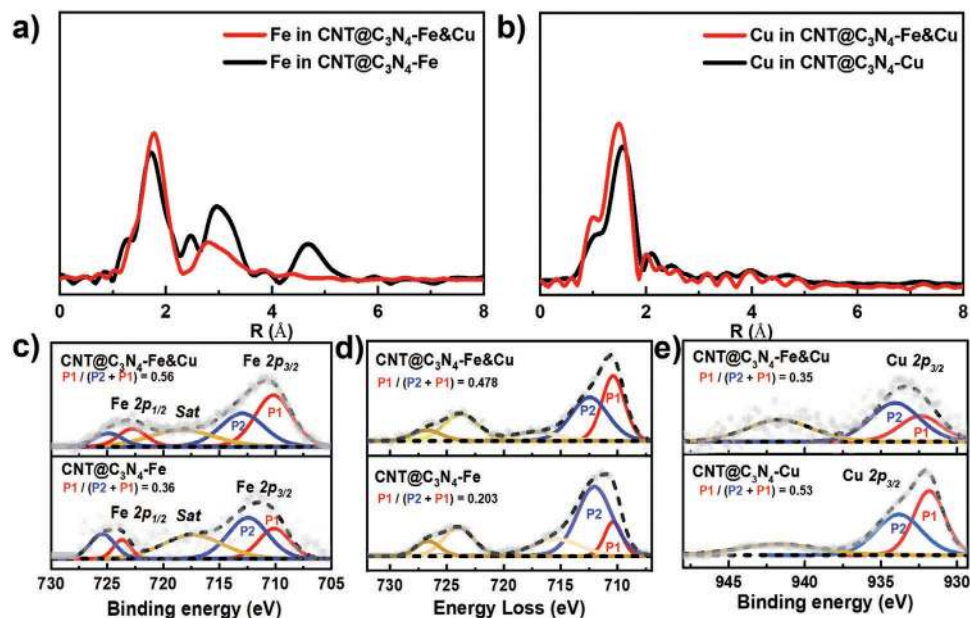

Figure 3. Chemistry analysis of the metal species in the materials. a) k^3-weighted EXAFS R-space spectrum of CNT@C_3N_4–Fe and CNT@C_3N_4–Fe&Cu; b) k^3-weighted EXAFS R-space spectra of CNT@C_3N_4–Cu and CNT@C_3N_4–Fe&Cu; c) deconvoluted high-resolution Fe 2p XPS spectra of CNT@C_3N_4–Fe&Cu and CNT@C_3N_4–Fe; d) deconvoluted Fe L-edge EELS spectra of CNT@C_3N_4–Fe&Cu and CNT@C_3N_4–Fe, with the ratio of low-valence Fe in the material; and e) deconvoluted high-resolution Cu 2p XPS spectra of CNT@C_3N_4–Fe&Cu and CNT@C_3N_4–Cu.

Figure S11, Supporting Information) was conducted to acquire more structural information. The first coordinate shell is well separated and analyzed, and the structure parameters are listed in Table S1 (Supporting Information). As shown, the coordinate numbers of the metal atoms in CNT@C$_3$N$_4$–Fe&Cu, CNT@C$_3$N$_4$–Fe, and CNT@C$_3$N$_4$–Cu are all larger the respective metal atoms in CuPc and FePc, implying the coordination between metal–metal atoms in addition to with nitrogen. Besides, the coordinate numbers of Fe and Cu in CNT@C$_3$N$_4$–Fe&Cu are also respectively higher than the values for CNT@C$_3$N$_4$–Fe and CNT@C$_3$N$_4$–Cu, which also suggests the higher ratio of metal–metal coordination in CNT@C$_3$N$_4$–Fe&Cu than in the CNT@C$_3$N$_4$–Fe and CNT@C$_3$N$_4$–Cu materials. Moreover, the CNT@C$_3$N$_4$–Fe&Cu also demonstrates a larger distance in the first shell than FePc and CuPc, which can be ascribed to the larger bond length in the Fe–Fe or Fe–Cu coordination condition, as shown in Figure S11 (Supporting Information). The average bond length (2.12 Å for Fe and 2.01 Å for Cu) is smaller than the theoretical average values in the proposed Fe&Cu cluster model (2.20 Å for Fe and 2.16 Å for Cu) but still larger than the typical values of FePc and CuPc, i.e., the single-atom Fe and Cu species. This indicates that the metal species in the material exist as a mixture of both metal clusters and singles, and this is also in agreement with the TEM observations (Figure 2).

The fine chemical states of these elements were then investigated by high-resolution XPS (Figure 3c; Figures S10 and S11, Supporting Information). As for the N1s spectra of all metal-doped CNT@C$_3$N$_4$ materials, nitrogen species bound with metal can be found; but no carbon–metal bonds are seen in their C1s spectra (Figures S10 and S11, Supporting

Information), further confirming local metal–nitrogen coordination in these reactors (Figure 1a).[33] Fe spectra contains three species at 710.4 eV (Fe 2p$_{3/2}$), 717 eV (satellite peak), and 723 eV (Fe 2p$_{1/2}$, Figure 3c).[34] Both the Fe 2p$_{3/2}$ and Fe 2p$_{1/2}$ can be deconvoluted into two peaks, corresponding to the Fe^{2+} (P1) and Fe^{3+} (P2) species. Compared with CNT@C$_3$N$_4$–Fe, the Fe^{2+} species in CNT@C$_3$N$_4$–Fe&Cu takes up a higher portion (0.56 vs 0.36), which indicates a lower oxidation state of Fe in CNT@C$_3$N$_4$–Fe&Cu. This is also in alignment with the deconvoluted EELS results showing a similar trend (Figure 3d).[34,35] In contrast, the oxidation state of Cu in CNT@C$_3$N$_4$–Fe&Cu increases compared with CNT@C$_3$N$_4$–Cu, as evidenced by the positive shift of the deconvoluted peaks with a higher portion of Cu^{2+} (Figure 3e).[36] This is in good agreement with the above XANES results and indicates the charge transfer between Cu and Fe, presenting an electron-rich and electron-deficient feature of the Fe and Cu atoms hosted in these subnano reactors.

The electrocatalytic NRR activity of the materials was assessed by chronoamperometry (CA),[37] and the ammonia production was determined by the indophenol blue method, with the absorb peak centered at around 650 nm (**Figure 4**a; Figures S12–S19, Supporting Information).[16] First, the origin of the produced ammonia was verified to eliminate the possible interference from the g-C$_3$N$_4$ host or other contaminations (Figure 4a). Specifically, CNT@C$_3$N$_4$, without any metal atom dopants, shows the same yet negligible NRR activity as pristine CNT under N$_2$ atmosphere, suggesting that g-C$_3$N$_4$ does not virtually affect or involve in the NRR process and no ammonia contamination from the N$_2$ feeding gas in our study. Meanwhile, ammonia was only detected when CNT@C$_3$N$_4$-Fe&Cu was tested under
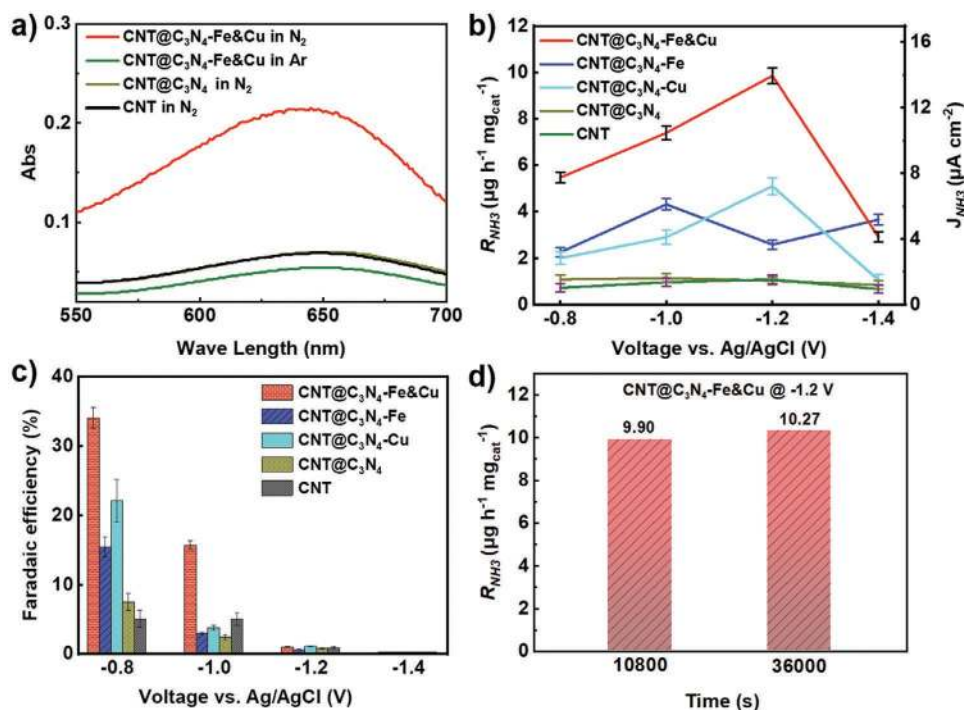

Figure 4. The electrocatalytic performance of the materials. a) UV–vis absorption spectra of various electrolytes stained with salicylic acid indicator; b) NH$_3$ yield rate and partial current densities of the materials at different potentials; c) the Faradaic efficiencies of the materials at different potentials; and d) The ammonia yield rate for 3 and 10 h tests at −1.2 V.

**ADVANCED
SCIENCE NEWS**

www.advancedsciencenews.com

**ADVANCED
MATERIALS**

www.advmat.de

N_2 rather than Ar, which suggests that the detected ammonia was from the reduced N_2. Comprehensively, these results have clearly confirmed that the origin of ammonia is from the NRR electrocatalysis, and neither g-C_3N_4 nor other impurities in the N_2 gas affected the ammonia yield in this study.

Afterward, the NRR performance of CNT@C_3N_4–Fe&Cu and analogs was studied and illustrated in Figure 4 and Figures S12–S19 (Supporting Information). Generally, the ammonia yield over the materials first increases and then decreases with the increase of overpotential. Among the analog materials, CNT@C_3N_4–Fe&Cu shows the highest ammonia yield (R_{NH3}, 9.86 µg mg^{-1} h^{-1}, Figure 4b). In comparison, the CNT@C_3N_4–Fe and CNT@C_3N_4–Cu are far inferior, as indicated by their much smaller R_{NH3}, which is, however, still better than the comparative CNT@N–Fe with isolated single atom centers (Figure S18, Supporting Information).

Faradaic efficiency (FE), representing the energy efficiency during the electrocatalysis process, was then calculated (Figure 4c), which decreases with the increase of the overpotential, due to the competitive hydrogen reduction reaction (HER).[38] Again, CNT@C_3N_4–Fe&Cu shows the highest value, which reaches the peak value at –0.8 V, corresponding to a FE of 34.0%, significantly higher than that of CNT@C_3N_4–Cu (22.0%) and CNT@C_3N_4–Fe (15.3%) at the same potential. To further study the relationship between competitive HER and Faradic efficiency, the HER performance of the materials was evaluated in a potential range from –0.6 to –1.6 V versus Ag/AgCl (Figure S23, Supporting Information). The CNT@C_3N_4–Fe&Cu demonstrates a similar current with CNT and CNT@C_3N_4, which is much lower than the current delivered by CNT@C_3N_4–Cu and CNT@C_3N_4–Fe, indicating the binary nanoreactor delivers a significantly lower activity for HER and consistent with its highest nitrogen reduction efficiency.

As a critical quality for electrocatalysts, the stability of electrocatalysis for CNT@C_3N_4–Fe&Cu was then evaluated (Figure 4d; Figures S19 and S22, Supporting Information). Over the 10 h test at –1.2 V, CNT@C_3N_4–Fe&Cu still presents a stable current of –1.6 mA and an ammonia yield rate of 10.27 µg mg^{-1} h^{-1}, which is on the same level for the 3 h test (–1.6 mA and 9.86 µg mg^{-1} h^{-1}), clearly showing its excellent durability during the long term electrocatalysis.

To better understand the performance enhancement from constructing such subnano reactors with multiple metal atoms, first principle calculations under the scheme of spin-polarized density functional theory have been performed, focusing on the synergetic effect of multiple metal centers. Specifically, we compared the NRR performance of the subnano reactors hosting triple metal atoms of dual types (i.e., both Fe and Cu) with those hosting triple metal atoms of one type (i.e., Fe or Cu) and the conventional "single-atom" ones with only one metal atom center (**Figure 5**; Figure S20, Supporting Information).

As determined by the cavity size of the g-C_3N_4 (Figure 5a), configuration with three metal atoms trapped in each cavity has been identified as the most stable, forming Cu_3, $CuFe_2$, and Fe_3 clusters. In this configuration, each metal atom is actually coordinated with two nitrogen-atoms and two metals, forming the 4-coordination configuration, which is in accordance with the aforementioned XANES, XPS, and EELS results. When an N_2 molecule is adsorbed on such subnano reactors with triple

metal atoms, as shown in Figure 5b, it is simultaneously stabilized by three metal atoms, rather than by one individual metal atom. As a result, it would not necessarily require the very strong N-metal bond as in the case of isolated sites (Figure S20a, Supporting Information) and thus the subsequent NH_3 desorption can be achieved with a lower energy input and thus effectively facilitated. This can be clearly verified by the calculated profiles of free energy changes (ΔG) for the elementary steps (Figure 5c–e; Figure S20b,c, Supporting Information). All of the subnano reactors with triple metal atoms offer higher activity as indicated by their smaller maximum ΔG (ΔG_{max} of 0.71 eV for Fe_3, 0.86 eV for Cu_3, and 0.58 eV for $CuFe_2$, Figure 5c–e) than those of single-atom catalytic centers (i.e., 1.72 eV for Cu and 1.73 eV for Fe, Figure S20, Supporting Information), indicating the much lower NRR barrier on these subnano reactors.

Moreover, on the subnano reactors with both Fe and Cu, the potential-determining step (PDS) for NRR is also significantly altered compared with the other two materials, indicating that the co-exitance of Cu and Fe sites have essentially different capacity to catalyze NRR. Specifically, the combination of Fe–Cu leads to optimal interaction with N_2, due to the stronger Fe—N bonding than N—Cu, which turns the PDS from the 5th hydrogenation (NH* → NH_2*) for CNT@C_3N_4–Fe (ΔG = 0.71 eV, Figure 5c) and the N_2 adsorption for CNT@C_3N_4–Cu (ΔG = 0.86 eV, Figure 5d), respectively, to the initial hydrogenation (N_2* → N_2H*) with a lower energy barrier (ΔG = 0.58 eV) for CNT@C_3N_4–Fe&Cu (Figure 5e). Besides, in the case of dual-metal reactor, the Cu atoms might act as a "cache" to supply electrons to the Fe center through the metal–metal coordination, as evidenced by the surface electronic structure characterizations showing the electron-rich feature of Fe atoms (Figure 3c,d); and the metal–metal coordination between Fe and Cu is also more efficient for electron transfer compared with the typical metal–N coordination in the conventional single-atom electrocatalysts. Consequently, these features collaboratively contribute to the enhanced NRR activity for CNT@C_3N_4–Fe&Cu in comparison with those with mono metal species or single-atom catalytic centers.

In summary, for the first time, we have demonstrated the utilization of the ordered subnano space in the surface cavities of g-C_3N_4 to host multiple Fe and Cu atoms, forming subnano reactors, as an efficient electrocatalyst for NRR. Due to the strong coordination among Fe and Cu atoms, which are intimately confined in such reactors, a significant synergy between these two species has been achieved, leading to significantly enhanced NRR performance in terms of high ammonia yield and efficiency that are much higher in comparison with the monometal counterparts. First principle calculations reveal that the coordination between Cu and Fe in this subnano reactor could simultaneously accelerate the adsorption of N_2 reactant and optimize the reaction pathway toward a lower energy barrier, leading to exceptionally facilitated NRR. Due to these outstanding features, it is expected that the CNT@C_3N_4–Fe&Cu material will be a very suitable catalyst for ammonia production under mild conditions and with low costs, and the concept of constructing subnano reactors should also shed light on the design of novel catalysts with a precision spatial location at subnanometer scale for a wide spectrum of catalytic reactions as well.
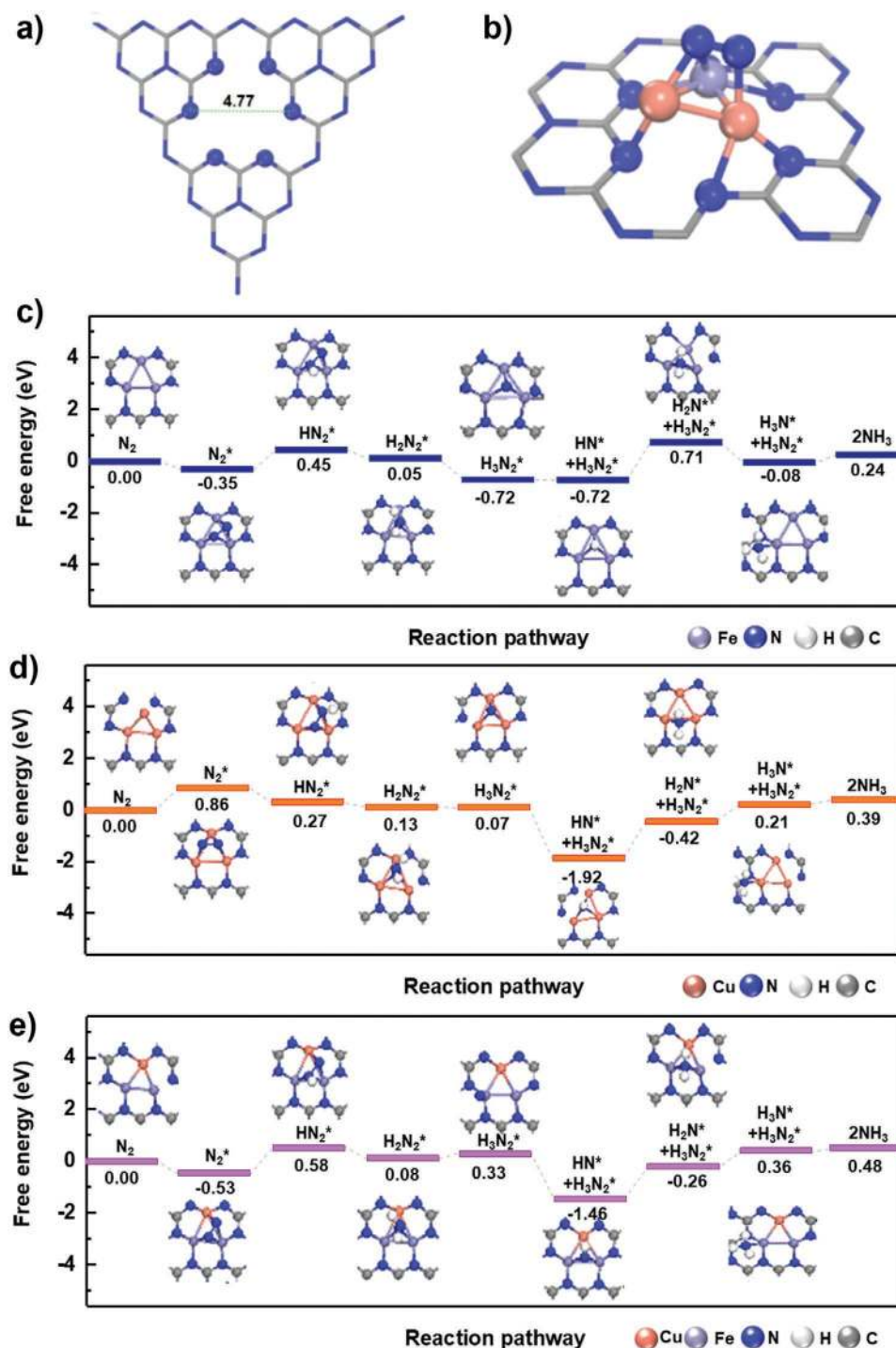
Figure 5. Calculated free energy profiles (ΔG) for elementary steps involved in NRR for catalysts. a) The basic unit of g-C$_3$N$_4$ with in-plain cavity size indicated in the unit of Å; b) adsorption configuration of an N$_2$ molecule over an atomic reactor with three metal atoms; and c–e) free energy diagrams of NRR on Fe$_3$ (c), Cu$_3$ (d), and Fe$_2$Cu (e) clusters in the cavity of g-C$_3$N$_4$. The structures of reaction intermediates are shown next to their energy segments.

Supporting Information

Supporting Information is available from the Wiley Online Library or from the author.

Acknowledgements

Conflict of Interest

The authors declare no conflict of interest.

Keywords

[1] a) I. Coric, B. Q. Mercado, E. Bill, D. J. Vinyard, P. L. Holland, *Nature* **2015**, *526*, 96; b) S. Licht, B. Cui, B. Wang, F. F. Li, J. Lau, S. Liu, *Science* 637, **2014**, *345*; c) T. Spatzal, K. A. Perez, O. Einsle, J. B. Howard, D. C. Rees, *Science* 1620, **2014**, *345*; d) T. Oshikiri, K. Ueno, H. Misawa, *Angew. Chem., Int. Ed. Engl.* **2016**, *55*, 3942.
[2] a) M. Kitano, Y. Inoue, Y. Yamazaki, F. Hayashi, S. Kanbara, S. Matsuishi, T. Yokoyama, S. W. Kim, M. Hara, H. Hosono, *Nat. Chem.* 934, **2012**, *4*; b) C. J. van der Ham, M. T. Koper, D. G. Hetterscheid, *Chem. Soc. Rev.* **2014**, *43*, 5183; c) M. Appl, *Ullmann's Encyclopedia of Industrial Chemistry*, Wiley-VCH, Weinheim, Germany **2006**.
[3] J. G. Chen, R. M. Crooks, L. C. Seefeldt, K. L. Bren, R. M. Bullock, M. Y. Darensbourg, P. L. Holland, B. Hoffman, M. J. Janik, A. K. Jones, *Science* **2018**, *360*, eaar6611.
[4] a) L. F. G. Julie N. Renner, A. M. Herring, K. E. Ayers, *Electrochem. Soc. Interface* **2015**, *24*, 51; b) S. P. S. B. S. Giddey, A. Kulkarni, *Int. J. Hydrogen Energy* **2013**, *38*, 14576.
[5] a) H. Cheng, P. Cui, F. Wang, L. X. Ding, H. Wang, *Angew. Chem., Int. Ed.* **2019**, *58*, 15541; b) G.-F. Chen, X. Cao, S. Wu, X. Zeng, L.-X. Ding, M. Zhu, H. Wang, *J. Am. Chem. Soc.* **2017**, *139*, 9771.
[6] V. Kordali, G. Kyriacou, C. Lambrou, *Chem. Commun.* **2000**, *17*, 1673.
[7] a) J. Wang, L. Yu, L. Hu, G. Chen, H. Xin, X. Feng, *Nat. Commun.* **2018**, *9*, 1795; b) M. M. Shi, D. Bao, S. J. Li, B. R. Wulan, J. M. Yan, Q. Jiang, *Adv. Energy Mater.* **2018**, *8*, 1800124.
[8] a) D. Bao, Q. Zhang, F. L. Meng, H. X. Zhong, M. M. Shi, Y. Zhang, J. M. Yan, Q. Jiang, X. B. Zhang, *Adv. Mater.* **2017**, *29*, 1604799; b) S. J. Li, D. Bao, M. M. Shi, B. R. Wulan, J. M. Yan, Q. Jiang, *Adv. Mater.* **2017**, *29*, 1700001; c) M. M. Shi, D. Bao, B. R. Wulan, Y. H. Li, Y. F. Zhang, J. M. Yan, Q. Jiang, *Adv. Mater.* **2017**, *29*, 1606550.
[9] S. Chen, S. Perathoner, C. Ampelli, C. Mebrahtu, D. Su, G. Centi, *Angew. Chem., Int. Ed. Engl.* **2017**, *56*, 2699.
[10] Y. Tong, H. Guo, D. Liu, J. Liang, X. Yan, P. Su, S. Zhou, J. Liu, G. Q. M. Lu, S. X. Dou, *Angew. Chem., Int. Ed.* **2020**, *59*, 7356.
[11] H. Li, J. Shang, Z. Ai, L. Zhang, *J. Am. Chem. Soc.* **2015**, *137*, 6393.
[12] A. Banerjee, B. D. Yuhas, E. A. Margulies, Y. Zhang, Y. Shim, M. R. Wasielewski, M. G. Kanatzidis, *J. Am. Chem. Soc.* **2015**, *137*, 2030.
[13] L. Zhang, L. X. Ding, G. F. Chen, X. Yang, H. Wang, *Angew. Chem., Int. Ed.* **2019**, *131*, 2638.
[14] C. Lv, Y. Qian, C. Yan, Y. Ding, Y. Liu, G. Chen, G. Yu, *Angew. Chem., Int. Ed.* **2018**, *57*, 10246.
[15] Q. Li, L. He, C. Sun, X. Zhang, *J. Phys. Chem. C* **2017**, *121*, 27563.
[16] H. Cheng, L. X. Ding, G. F. Chen, L. Zhang, J. Xue, H. Wang, *Adv. Mater.* **2018**, *30*, 1803694.
[17] a) L. M. Azofra, N. Li, D. R. MacFarlane, C. Sun, *Energy Environ. Sci.* 2545, **2016**, *9*; b) Y. Luo, G. F. Chen, L. Ding, X. Chen, L. X. Ding, H. Wang, *Joule* **2019**, *3*, 279.
[18] J. Zhao, Z. Chen, *J. Am. Chem. Soc.* **2017**, *139*, 12480.
[19] a) C. Liu, Q. Li, C. Wu, J. Zhang, Y. Jin, D. R. MacFarlane, C. Sun, *J. Am. Chem. Soc.* **2019**, *141*, 2884; b) C. Ling, X. Niu, Q. Li, A. Du, J. Wang, *J. Am. Chem. Soc.* **2018**, *140*, 14161.
[20] Z. Chen, J. Zhao, C. R. Cabrera, Z. Chen, *Small Methods* **2018**, *3*, 1800368.
[21] Z. Geng, Y. Liu, X. Kong, P. Li, K. Li, Z. Liu, J. Du, M. Shu, R. Si, J. Zeng, *Adv. Mater. 30*, **2018**, 1803498.
[22] a) M. W. Haynes, *CRC Handbook of Chemistry and Physics*, CRC Press, Boca Raton, FL, USA **2010**; b) A. W. X. F. Yang, B. Qiao, J. Li, J. Liu, T. Zhang, *Acc. Chem. Res.* **2013**, *46*, 1740; c) J. Huang, J. Chen, T. Yao, J. He, S. Jiang, Z. Sun, Q. Liu, W. Cheng, F. Hu, Y. Jiang, Z. Pan, S. Wei, *Angew. Chem., Int. Ed.* **2015**, *54*, 8722; d) X. Li, W. Bi, M. Chen, Y. Sun, H. Ju, W. Yan, J. Zhu, X. Wu, W. Chu, C. Wu, Y. Xie, *J. Am. Chem. Soc.* **2017**, *139*, 14889; e) J. Wang, Z. Huang, W. Liu, C. Chang, H. Tang, Z. Li, W. Chen, C. Jia, T. Yao, S. Wei, Y. Wu, Y. Li, *J. Am. Chem. Soc.* **2017**, *139*, 17281; f) X. Li, W. Bi, M. Chen, Y. Sun, H. Ju, W. Yan, J. Zhu, X. Wu, W. Chu, C. Wu, Y. Xie, *J. Am. Chem. Soc.* **2017**, *139*, 14889.
[23] a) S. Sun, G. Zhang, N. Gauquelin, N. Chen, J. Zhou, S. Yang, W. Chen, X. Meng, D. Geng, M. N. Banis, *Sci. Rep.* **2013**, *3*, 1775; b) H. Yan, H. Cheng, H. Yi, Y. Lin, T. Yao, C. Wang, J. Li, S. Wei, J. Lu, *J. Am. Chem. Soc.* **2015**, *137*, 10484; c) H. J. Qiu, Y. Ito, W. Cong, Y. Tan, P. Liu, A. Hirata, T. Fujita, Z. Tang, M. Chen, *Angew. Chem., Int. Ed.* **2015**, *54*, 14031.
[24] Y. Zheng, Y. Jiao, Y. Zhu, Q. Cai, A. Vasileff, L. H. Li, Y. Han, Y. Chen, S. Z. Qiao, *J. Am. Chem. Soc.* **2017**, *139*, 3336.
[25] L. Chade, Q. Yumin, Y. Chunshuang, D. Yu, L. Yuanyue, C. Gang, Y. Guihua, *Angew. Chem., Int. Ed.* **2018**, *57*, 10246.
[26] X. Guo, J. Gu, S. Lin, S. Zhang, Z. Chen, S. Huang, *J. Am. Chem. Soc.* **2020**, *142*, 5709.
[27] a) Z. Lu, B. Wang, Y. Hu, W. Liu, Y. Zhao, R. Yang, Z. Li, J. Luo, B. Chi, Z. Jiang, M. Li, S. Mu, S. Liao, J. Zhang, X. Sun, *Angew. Chem., Int. Ed.* **2019**, *58*, 2622; b) H. Yan, Y. Lin, H. Wu, W. Zhang, Z. Sun, H. Cheng, W. Liu, C. Wang, J. Li, X. Huang, T. Yao, J. Yang, S. Wei, J. Lu, *Nat. Commun.* **2017**, *8*, 1070.
[28] a) H. Tian, J. Liang, J. Liu, *Adv. Mater.* **2019**, *31*, 1903886; b) A. Studer, D. P. Curran, *Nat. Chem.* **2014**, *6*, 765.
[29] S. Sadjadi, S. Sadjadi, *Supramolecular Coordination Cages as Nanoreactors in Organic Nanoreactors*, Academic Press, San Diego, CA, USA **2016**.
[30] a) R. Chen, J. Zhang, Y. Wang, X. Chen, J. A. Zapien, C.-S. Lee, *Nanoscale* **2015**, *7*, 17299; b) G. P. Mane, D. S. Dhawale, C. Anand, K. Ariga, Q. Ji, M. A. Wahab, T. Mori, A. Vinu, *J. Mater. Chem. A* **2013**, *1*, 2913; c) J. Fang, H. Fan, Z. Zhu, L. B. Kong, L. Ma, *J. Catal.* **2016**, *339*, 93.
[31] W. Klement, *Trans. Metall. Soc. AIME* **1965**, *233*, 1180.
[32] a) A. Thomas, A. Fischer, F. Goettmann, M. Antonietti, J. O. Müller, R. Schlögl, J. M. Carlsson, *J. Mater. Chem. A* **2008**, *18*, 4893; b) D. Pease, S. Bader, M. Brodsky, J. Budnick, T. Morrison, N. Zaluzec, *Phys. Lett. A* 491, **1986**, *114*; c) R. Leapman, L. Grunes, P. Fejes, *Phys. Rev. B* **1982**, *26*, 614; d) J. H. Paterson, O. L. Krivanek, *Ultramicroscopy* **1990**, *32*, 319.
[33] W. Ju, A. Bagger, G.-P. Hao, A. S. Varela, I. Sinev, V. Bon, B. R. Cuenya, S. Kaskel, J. Rossmeisl, P. Strasser, *Nat. Commun.* **2017**, *8*, 1.
[34] S. Srivastava, S. Badrinarayanan, A. J. Mukhedkar, *Polyhedron* **1985**, *4.3*, 409.

[35] G. C. Allen, M. T. Curtis, A. J. Hooper, P. M. Tucker, *J. Chem. Soc., Dalton Trans.* **1974**, 1525.

[36] a) V. Nefedov, Y. V. Salyn, P. Solozhenkin, G. Y. Pulatov, *Surf. Interface Anal.* **1980**, *2*, 170; b) N. McIntyre, M. Cook, *Anal. Chem.* **1975**, *47*, 2208.

[37] H. Mikosch, E. Uzunova, G. Nikolov, *J. Phys. Chem. B* **2005**, *109*, 11119.

[38] a) H. Cheng, L. X. Ding, G. F. Chen, L. Zhang, J. Xue, H. Wang, *Adv. Mater.* **2018**, *30*, 1803694; b) H. Mikosch, E. L. Uzunova, G. St. Nikolov, *J. Phys. Chem. B* **2005**, *109*, 11119.